Geochim. Cosmochim. Acta 57, 4301 (1993); G. Ravizza, Earth Planet. Sci. Lett. 118, 335 (1993); B. Peucker-Ehrenbrink, G. Ravizza, A. W. Hoffmann, ibid. 130, 155 (1994).

10. G. Ravizza and K. K. Turekian, Earth Planet. Sci. Lett. 110, 1 (1992).
11. An increasing concentration over time could be interpreted as the result of a loss of tracer into the inner face of the Teflon vessel. In order to eliminate this possibility, 4 ml of CTD4-6 was analyzed with the procedure that was developed in (4), which is usually used for a wide variety of rock samples of small weight (without the dissolution step—H_2SO_4 was used instead of HNO_3). The measured [Os] was 10.2 ± 0.7, and the $^{187}Os/^{186}Os$ ratio was 8.6 ± 0.5 (the values were corrected from the blank), implying that there was no measurable differential loss of tracer or sample.
12. D. G. Brookins, Eh-pH Diagrams for Geochemistry (Springer-Verlag, New York, 1988), pp. 92–93; F. G. Cotton and G. Wilkinson, Advanced Inorganic Chemistry (Wiley, Chichester, UK, ed. 5, 1988).
13. W. M. Sackett, in Chemical Oceanography, J. P. Riley and R. Chester, Eds. (Academic Press, London, 1978), pp. 127–172.
14. B. K. Esser and K. K. Turekian, Geochim. Cosmochim. Acta 57, 3093 (1993).
15. C. J. Allègre and J.-M. Luck, Earth Planet. Sci. Lett. 48, 148 (1980).
16. A. Krogh and A. Keys, Biol. Bull. 67, 132 (1934); J. H. Sharp, Mar. Chem. 56, 265 (1997).
17. G. S. Jacinto and C. M. G. Van den Berg, Nature 338, 332 (1989); A. D. Anbar, G. J. Wasserburg, D. A. Papanastassiou, P. S. Andersson, Science 273, 1524 (1996) and references therein.
18. B. Peucker-Ehrenbrink and G. Ravizza, Geology 24, 327 (1996); K. W. Burton et al., J. Conf. Abstr. 1, 92 (1996).
19. A few results were obtained by M. Sharma and G. J. Wasserburg [Geochim. Cosmochim. Acta 61, 5411 (1997)] with the same technique that was used to estimate the Os concentration in seawater. The data used here are our unpublished results from samples of several other major rivers, whose concentrations range from 5 to 25 pg/kg.
20. The residence time estimate is made with the assumption that the Os river input to the ocean is only 80% of the total input (2).
21. We thank the team of the EDUL mission, especially C. Mével, who agreed to sample seawater for us on an already scheduled mission, and A. Dappoigny, who performed the sampling. We also thank K. W. Burton for helpful discussions. This is Institut de Physique du Globe de Paris contribution 1565.

1 July 1998; accepted 4 September 1998

Experimental Demonstration of Guiding and Bending of Electromagnetic Waves in a Photonic Crystal

Shawn-Yu Lin,* Edmund Chow, Vince Hietala, Pierre R. Villeneuve, J. D. Joannopoulos

The routing and interconnection of optical signals through narrow channels and around sharp corners are important for large-scale all-optical circuit applications. A recent computational result suggests that photonic crystals may offer a novel way of achieving this goal by providing a mechanism for guiding light that is fundamentally different from traditional index guiding. Waveguiding in a photonic crystal and near 100 percent transmission of electromagnetic waves around sharp 90 degree corners were observed experimentally. Bending radii were made smaller than one wavelength.

The efficient guiding and interconnection of light on a chip are important for telecommunication and optical computing applications (*1*, *2*). Conventional dielectric waveguides can support guided modes along straight lines with high efficiency yet are restricted by radiation loss to a moderate bending radius (*3*). A recent theoretical investigation suggests that photonic crystals hold the key for overcoming this problem. It is predicted that a photonic crystal waveguide can guide light with great efficiency either along a straight path (*4*) or around a sharp corner (*5–7*). It is further suggested that light can be guided in air, minimizing guiding loss due to material absorption.

Photonic crystals, also known as photonic band gap (PBG) materials, are artificially engineered dielectric materials that exhibit a frequency regime over which propagation of light is strictly forbidden (*8*). A linear defect in a photonic crystal can give rise to a band of defect states within the gap and act as a waveguide (see Fig. 1A). Light in the photonic crystal is confined to and guided along the one-dimensional (1D) channel because the gap forbids light from escaping into the bulk crystal. A waveguide bend (Fig. 1B) can then steer light around a sharp 90° corner. A simple scattering theory predicts the existence of reflection nodes where 100% transmission efficiency can be achieved through the bend (*5*). We now demonstrate waveguiding of electromagnetic (EM) waves by a PBG line defect and, more importantly, observe near perfect transmission of EM waves around a sharp corner in a photonic crystal.

The two-dimensional (2D) photonic crystal we used to construct straight waveguides and waveguide bends consisted of a square array of circular Alumina rods having a dielectric constant, ε, of 8.9 and a radius, r, of $0.20a$, where a is the lattice constant of the square array. In our experiment, the lattice constant was chosen to be 1.27 mm. For such a 2D photonic crystal, a large photonic band gap exists for light polarized parallel to the rods that extends from a frequency of $0.32c/a$ (76 GHz) to $0.44c/a$ (105 GHz). Here, c is the speed of light.

A line defect is created inside the crystal by removing a row of rods. The line defect introduces an optical mode inside the crystal. Its localization strength depends on the specific modal frequency; at midgap, the guided mode extends less than one-half of a wavelength into the crystal (*9*). The translational symmetry along the line defect allows the guided mode to be described with two quantum numbers: frequency (f) and wave vector ($\mathbf{k}$). A f versus $\mathbf{k}$ dispersion relation uniquely characterizes the propagation of light in the waveguide. Computed results of such a dispersion relation along the high-symmetry crystal direction <10> are shown in Fig. 2, along with the extent of the PBG. The dispersion is strongly nonlinear near the cutoff at $\mathbf{k} = 0$. It becomes linear at higher frequencies and eventually intercepts the upper branch of the photonic band gap at $f = 0.44\ c/a$. The bandwidth Δf of the guided mode is very large and extends over the entire width of the band gap. Had we chosen a lattice constant, a, of 0.59 μm (infrared regime) instead of 1.27 mm (millimeter-wave regime), the band gap would have been centered at a wavelength $\lambda = 1.55$ μm, and the guided-mode bandwidth $\Delta\lambda$ would have extended over a range of 430 nm.

To test the PBG waveguides, we used a HP8510C millimeter-wave source unit with a tunable frequency range from 75 to 110 GHz. The electric field of the emitted EM wave was polarized parallel to the dielectric rods and was coupled into the PBG waveguide with two metallic millimeter-wave waveguides, a transmitter and a receiver, placed next to the entrance and exit respectively, of the PBG waveguide. This scheme was used to optimize coupling into the PBG waveguide. It closely mirrors the setup used in the computational simulations (*5*). In the simulations, a point dipole, acting as a transmitter, was placed at the entrance of the PBG waveguide, and the field amplitude was monitored at a point located inside the guide

S.-Y. Lin, E. Chow, V. Hietala, Sandia National Laboratories, Post Office Box 5800, Albuquerque, NM 87185, USA. P. R. Velleneuve and J. D. Johannopoulos, Department of Physics, Massachusetts Institute of Technology, Cambridge, MA 02139, USA.

*To whom correspondence should be addressed. E-mail: slin@sandia.gov

after the bend (receiver) (*5, 10*). In the ideal situation, the experimental setup would allow for complete coupling of light from the transmitter to the PBG waveguide.

The transmission spectrum of a straight PBG waveguide is shown in Fig. 3A. As expected, the PBG waveguide transmits light over a broad range of frequencies, from ~80 to ~105 GHz. The measured spectrum displays a strong f dependence; its peak is close to midgap, and transmission falls off near the band edges. The f dependence is attributed to mode-matching efficiency (that is, modal overlap) between the mode in the metallic waveguide and the one in the PBG waveguide. The best matching occurs near midgap, where the modes in both the metallic and PBG waveguides have a similar extent. Near the band edges, the guided mode extends more deeply into the crystal, and mode matching becomes poorer. Also, at the low-f band edge, the group velocity of the guided mode is near zero, making signal detection difficult at the output.

Another distinctive feature of the PBG waveguide is the localization of light in air, reducing signal loss due to material absorption. The only loss comes from a slight penetration of light into the photonic crystal, which is estimated to be ~10% of its modal volume at midgap frequencies. Compared with a ridge dielectric waveguide, signal loss is reduced by a factor of 10. By measuring and comparing transmission amplitude of guides with different lengths, the guiding loss of a straight waveguide is estimated to be 0.3 dB/cm over the entire band gap regime. PBG waveguides thus provide a natural solution to the self-absorption problem often encountered in planar integration of active lasers with passive waveguides. They are also more advantageous than metallic waveguides because metal waveguides undergo severe signal loss at optical wavelengths.

A PBG waveguide bend may be constructed by joining together three pieces of straight guides that are oriented along the <10>, <11>, and <01> directions, respectively. The <10> and <01> guides serve as input- and output-coupling waveguides, respectively. The <11> guide acts as an ultrasmall 45° mirror that bends the light. To test the device, we again placed the transmitter and receiver next to the entrance and exit of the PBG waveguides. The measured spectrum for the waveguide bend is shown in Fig. 3A with red circles. As expected, the amplitude through the bend is slightly smaller than that of the straight waveguide over the entire frequency range, with two exceptions; at f_1 ~87 GHz and f_2 ~101 GHz, both spectra have equal amplitudes, suggesting that zero loss transmission is observed through a 90° PBG bend. Moreover, the bending radius for this geometry is less than one wavelength, which constitutes the smallest radius ever achieved in any dielectric waveguide with complete transmission efficiency (*11*).

To obtain the intrinsic transmission efficiency of the PBG bend, we normalized the transmission spectrum through the bend to that of the straight waveguide. The normalized spectrum is shown in Fig. 3B. The PBG bend exhibits near perfect transmission at f_1 and f_2 (*12*). The two arrows indicate the expected position of the reflection nodes computed with the simple model presented in (*5*), which uses a single input parameter L that corresponds to the physical length of the PBG waveguide along the <11> direction. In the case presented above, L is equal to $2.33 \times \sqrt{2}a$. The solid red line is a polynomial fit of the data. The theo-

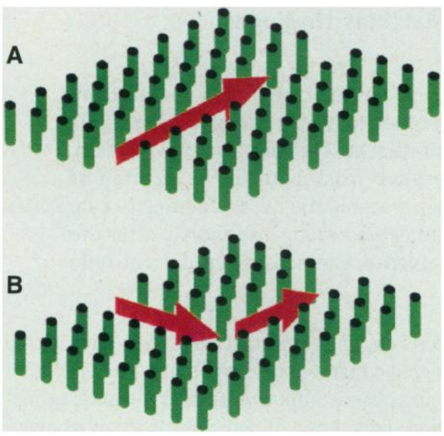

Fig. 1. (**A**) Schematic diagram of a photonic crystal straight waveguide. (**B**) Schematic diagram of a photonic crystal waveguide bend. The green rods are made of dielectric material. The red arrows indicate the direction of light flow.

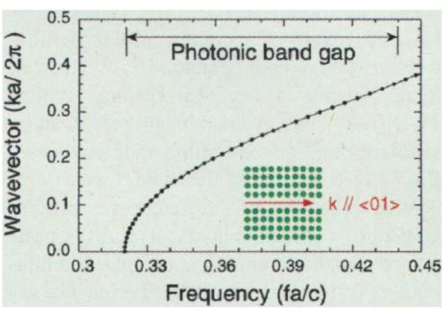

Fig. 2. Dispersion relation of the guided modes along a line defect in the <10> direction. Light propagates along the PBG channel according to the specific **k** versus f relation.

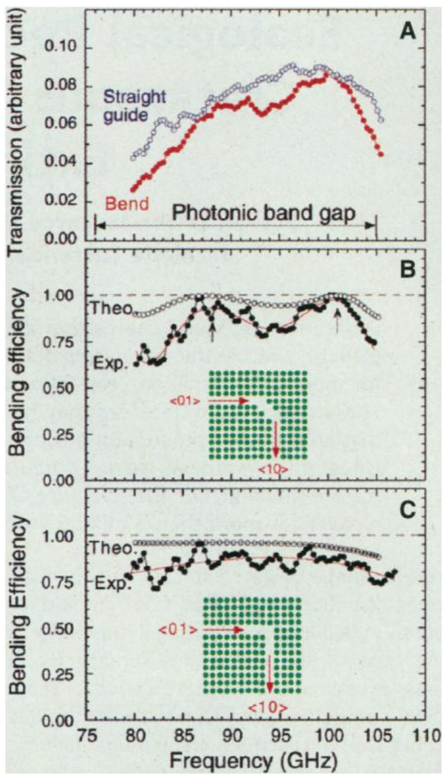

Fig. 3. (**A**) Transmission spectra for a straight waveguide (blue circles) and a waveguide bend (red circles) in a 2D photonic crystal. The amplitudes of the two curves are equal at frequencies f_1 ~87 GHz and f_2 ~101 GHz, suggesting zero loss transmission through the sharp 90° corner. (**B**) Bending efficiency as a function of frequency. The solid circles correspond to experimental data; the open circles are obtained from theory. Near perfect bending efficiency is observed around 87 and 101 GHz. The black arrows indicate the positions of the predicted peaks. The PBG bending geometry is shown in the inset. (**C**) Bending efficiency of a PBG waveguide bend with zero radius of curvature. High transmission exceeding 80% is observed. The open and solid circles correspond to theoretical and experimental data, respectively. The PBG bending geometry is shown in the inset. The red lines in (B) and (C) are polynomial fits to the data.

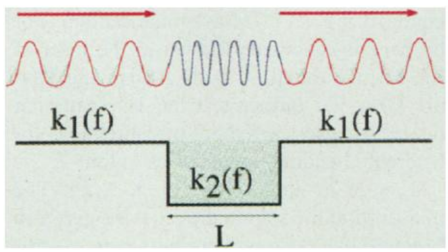

Fig. 4. Schematic diagram of the 1D scattering process. The <11> bending section is modeled as a scattering center (blue). Scattering arises from the wave vector mismatch between the <10> (red) and <11> sections. Complete forward scattering occurs when light propagating along the <10> direction is in resonance with the <11> bending section.

Table 1. Experimentally observed and computationally predicted transmission peaks for three different bending lengths L.

L	f_1 (GHz)		f_2 (GHz)	
	Theory	Experiment	Theory	Experiment
1.33	84.0	86 ± 3	105	102 ± 3
2.33	87.5	88 ± 3	101	101 ± 3
3.33	89.0	88 ± 3	99.0	99 ± 3

retical bending efficiency is also shown in Fig. 3B. The peaks in Fig. 3B confirm a subtle and important point about PBG waveguides. Indeed, the detection of light at the end of a straight waveguide would not be a sufficient condition, in itself, to confirm PBG guiding. It is the existence of transmission peaks around the sharp bend, along with the specific position of these peaks, that validates the model.

The position of the peaks can be predicted with a 1D scattering theory (*5*). The <11> bending section is modeled as a scattering center with a channel length L (Fig. 4). Light propagating along the <10> direction is scattered by the <11> section into the <01> direction. We label the wave vectors associated with the <10>, <11>, and <01> states as $\mathbf{k}_1(f)$, $\mathbf{k}_2(f)$, and $\mathbf{k}_1(f)$, respectively. The strength of the scattering is determined by the mismatch between $\mathbf{k}_1$ and $\mathbf{k}_2$. If the mismatch is small [the dispersion $\mathbf{k}(f)$ is close to being isotropic], forward scattering is favored, and high transmission efficiency is expected. Complete forward scattering occurs when a resonance inside the bend is established. At such a resonance, light travels freely through the bend with 100% efficiency.

Quantitatively, the reflection coefficient near the transmission peaks is given by $R(f) \cong 4 \times (\Delta\mathbf{k}/\mathbf{k})^2 \times [\sin(\mathbf{k}_2 L)]^2$, where $\Delta\mathbf{k} = (\mathbf{k}_1 - \mathbf{k}_2)/2$ is the wave vector mismatch and $\mathbf{k} = (\mathbf{k}_1 + \mathbf{k}_2)/2$ is the average wave vector. Resonance occurs when $\sin[(\mathbf{k}_2\ (f)\mathrm{L}] = 0$. The position of the transmission peaks can readily be obtained by computing the dispersion relation $\mathbf{k}_2(f)$ and by determining the length of the <11> waveguide section. For the bending geometry shown in the inset of Fig. 3B, we found f_1 = 87.5 GHz and f_2 = 101 GHz. To further test the 1D scattering theory, we also carried out measurements for different bending geometries with $L = 1.33 \times \sqrt{2}a$ and $L = 3.33 \times \sqrt{2}a$. The measured and computed peaks are given in Table 1. The agreement between experiment and theory is excellent confirmation of the validity of the 1D model, hence confirming the existence of guided modes in the photonic crystal.

The 1D model also predicts high transmission efficiency in PBG waveguides with zero radius of curvature. A schematic of the bending geometry is shown in Fig. 3C along with the experimental data. As predicted, the transmission spectrum does not display a series of peaks, yet it shows an overall transmission efficiency larger than 80%. This high transmission efficiency can be compared with ~30% transmission efficiency in similar high-index dielectric waveguides (*5*).

References and Notes

1. See, for example, C. Yeh, *Applied Photonics* (Academic Press, San Diego, CA, 1994).
2. C. Wu, *Science News* **150**, 309 (1996); G. Taubes, *Science* **278**, 1709 (1997).
3. E. A. J. Marcatili, *Bell Syst. Tech. J.* **48**, 2103 (1969).
4. J. D. Joannopoulos, R. D. Meade, J. N. Winn, *Photonic Crystals* (Princeton Univ. Press, New York, 1995).
5. A. Mekis *et al.*, *Phys. Rev. Lett.* **77**, 3787 (1996).
6. M. M. Sigalas *et al.*, in *Proceedings of the 14th Annual Review of Progress in Applied Computational Electromagnetics* (Applied Computational Electromagnetics Society, Monterey, CA), pp. 144–150.
7. J. D. Joannopoulos, P. R. Villeneuve, S. Fan, *Nature* **386**, 143 (1997).
8. E. Yablonovitch and T. J. Gmitter, *Phys. Rev. Lett.* **63**, 1950 (1989); K. M. Ho, C. T. Chan, C. M. Soukoulis, *ibid.* **65**, 3152 (1990); K. M. Leung and Y. F. Liu, *ibid.*, p. 2646; H. S. Sozuer and J. W. Haus, *J. Opt. Soc. Am. B* **10**, 296 (1993).
9. S. Y. Lin and G. Arjavalingam, *Opt. Lett.* **18**, 1666 (1993).
10. J. C. Chen and K. Li, *Microwave Opt. Technol. Lett.* **10**, 319 (1995).
11. To the best of our knowledge, even for a metallic millimeter-wave 90° waveguide bend, the best commercially available one has a bending radii of 4 to 5 wavelengths.
12. Our measurement is accurate to about ±5% mainly because of an amplitude oscillation caused by resonance between the input and output end of the PBG guide. Also, the absolute bending efficiency is slightly lower, ~3%, because the <10> and <01> sections of the bend would contribute to a small guiding loss.

13. The work at Sandia National Laboratories is supported through the U.S. Department of Energy under contract DE-AC04-94AL85000. Sandia is a multiprogram laboratory operated by Sandia Corporation, a Lockheed Martin Company, for the U.S. Department of Energy. The work at Massachusetts Institute of Technology is supported in part by the Material Research Science and Engineering Center program of the NSF under award DMR-9400334.

6 July 1998; accepted 10 September 1998

Organic Carbon Fluxes and Ecological Recovery from the Cretaceous-Tertiary Mass Extinction

Steven D'Hondt, Percy Donaghay, James C. Zachos, Danielle Luttenberg, Matthias Lindinger

Differences between the carbon isotopic values of carbonates secreted by planktic and benthic organisms did not recover to stable preextinction levels for more than 3 million years after the Cretaceous-Tertiary mass extinction. These decreased differences may have resulted from a smaller proportion of marine biological production sinking to deep water in the postextinction ocean. Under this hypothesis, marine production may have recovered shortly after the mass extinction, but the structure of the open-ocean ecosystem did not fully recover for more than 3 million years.

A wide range of geochemical evidence indicates that the organic flux from the surface ocean to the deep sea decreased drastically at the time of the Cretaceous-Tertiary (K-T) mass extinction and did not recover for more than a million years. The evidence for this collapse of the deep-sea organic flux includes dramatic decreases in (i) carbon isotopic (δ^{13}C) differences between carbonate skeletons secreted by planktic and benthic organisms (usually foraminifera) (*1–6*), (ii) δ^{13}C differences between benthic foraminiferal skeletons (tests) from different ocean basins (*2*), (iii) δ^{13}C differences between the tests of benthic foraminifera that lived on the seafloor and those that lived in the underlying sediment (*3*), and (iv) the accumulation of barium in deep-sea sediments (*3*).

Our study of planktic-to-benthic δ^{13}C differences indicates that final recovery of the organic flux to the deep sea may have occurred more than 3 million years after the mass extinction (Figs. 1 and 2). An early phase of recovery is marked by the return of planktic-to-benthic δ^{13}C differences (and interbenthic δ^{13}C differences) to low but relatively stable levels within the first several hundred thousand years after the extinction (*1–4*). This early stage of recovery has been identified at Pacific, Southern Ocean, and South Atlantic sites (*1–4*). After this early phase of recovery, differences between planktic and benthic δ^{13}C values at South Atlantic Deep Sea Drilling Project (DSDP) site 528 remained below preextinction levels for more than 2 million additional years (Fig. 2). At site 528, the final recovery of planktic-to-benthic δ^{13}C differences is exhibited by fine (<25 μm in diameter) $CaCO_3$, near-surface planktic foraminifera and planktic foraminifera that lived deeper in the thermocline (*7*) (Fig. 2). The parallel nature of these planktic-to-benthic records provides strong evidence that surface-to-deep δ^{13}C gradients did not fully recover for more than 3 million years after the

S. D'Hondt, P. Donaghay, D. Luttenberg, Graduate School of Oceanography, University of Rhode Island, Narragansett, RI 02882, USA. J. C. Zachos, Earth Sciences Department, University of California, Santa Cruz, CA 95064, USA. M. Lindinger, Rossinistrasse 5, D-88353 Kissligg, Germany.